

XXZ-Ising model on the triangular kagome lattice with spin-1 on the decorated trimers

Chengkang Zhou,¹ Yuanwei Feng,¹ Jiawei Ruan,^{1,2} and Dao-Xin Yao^{1,*}

¹State Key Laboratory of Optoelectronic Material and Technologies,
School of Physics, Sun Yat-sen University, Guangzhou 510275, China

²National Laboratory of Solid State Microstructures, School of Physics and Collaborative
Innovation Center of Advanced Microstructures, Nanjing University, Nanjing 210093, China.

(Dated: April 8, 2022)

We consider the triangular kagome XXZ-Ising model (TKL XXZ-Ising model) formed by inserting small triangles ("a-trimers") with XXZ spin-1 inside the triangles of the kagome lattice ("b-trimers"). It is a novel mixed spin system and can be solved exactly by transforming into the kagome lattice with the general transformation method for decorated spin systems. In the absence of an external field, we integrate out the quantum spins of the a-trimers and map the TKL model to the kagome Ising model exactly. We obtain the full phase diagram and their zero-temperature entropies (e.g. $s_{max} = 5.48895$ per unit cell is given for the phase with the maximum entropy). When an external field is applied, 20 phases are found due to the quantum fluctuations of a-trimers. Moreover, the high spins in the a-trimers can lead to a stable quantized growth of the magnetization process in the Heisenberg limit.

I. INTRODUCTION

Introducing quantum fluctuations into a classical model have both fundamental and practical importance for finding new quantum phases at low temperature. Specially, it can lead to a multitude of new quantum phases and transitions in frustrated systems with a large ground state degeneracy, for example the tetramer-dimer and dimer-monomer phases in the frustrated Heisenberg diamond chain[1], kagome loop gas in the triangle kagome lattice[2]. It is known that such unusual phases are the result of the interplay between quantum fluctuations and geometric frustrations[3]. Since the degenerate states in such systems have the same energy and all perturbations are singular, any linear combination of the classically degenerate states is a candidate for quantum ground state[4]. Hence, this effect plays an important role in frustrated mixed spin systems including both spin-1/2 and higher spins, which hold the possibility of the diversity of classically degenerate states.

Theoretical interest in mixed spin systems is increasing in recent years. Most of the mixed spin systems are constructed by inserting high spin decorated parts in the standard Ising spin systems. For instance, the high spin decorated parts in a diamond chain exhibits an outstanding diversity of magnetization properties[5]. Among them, the triangle kagome lattice (TKL) is a typical structure formed by inserting small triangles into the large triangles of the kagome lattice (as shown in FIG.1) instead of bond decorated parts. It was founded in $\text{Cu}_9\text{X}_2(\text{cpa})_6 \cdot x\text{H}_2\text{O}$ in the 1990s [6–9]. Previous researches[2, 6–17] have revealed that the TKL XXZ-Ising model with the spin-1/2 a-trimers inside the triangles of the kagome lattice can be solved exactly with the general transformation method for decorated spin system. However, in the presence of mixed odd-spin and even-spin, the TKL XXZ-Ising model calls for further investigations.

The general transformation method for decorated spin sys-

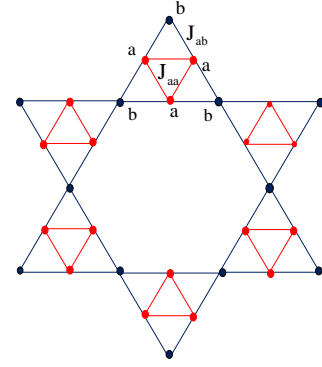


FIG. 1. The XXZ-Ising model of triangular kagome lattice (TKL) formed by introducing small triangles ("a-trimers", red) with XXZ spins on the kagome lattice ("b-trimers", blue) with Ising spins.

tems was first introduced by Fisher in the 1950s[18] and developed in recent years[19, 20]. It has been widely applied in studying the decorated spin system, in both one[21–23] and two[24–27] dimensions. With this method, the TKL XXZ-Ising model remains solvable when changing the decorated part with higher spins, serving as a candidate for observing the effects of quantum fluctuations in the mixed spin systems with geometric frustrations.

In this paper, we study the TKL XXZ-Ising model decorated by the spin-1 a-trimers (TKL spin-1 model) using the general transformation. And we find that the phase diagram gets more complicated as the spins of the decorated parts become higher. In addition, by observing the difference between spin-1/2 and spin-1 cases, we also obtain a picture of how the phase diagram of the TKL XXZ-Ising model evolves to its classical limit with higher spins in the a-trimers.

The rest of this paper is organized as follows. In Section II, we give the Hamiltonian of the TKL XXZ-Ising model decorated by the spin-1 a-trimers and introduce the transformation method. In section III, we discuss the zero temperature phase diagram without the external field and compare with the TKL spin-1/2 case. In section IV, we present the zero tempera-

* Corresponding author: yaodaox@mail.sysu.edu.cn

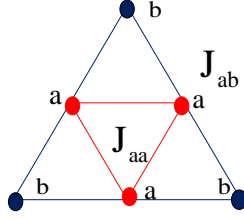


FIG. 2. A hexamer contains three spins on the a-sublattice and three spins on the b-sublattice. Each b-spin is shared by two hexamers

ture phase diagram in the presence of a finite magnetic field and discuss the effect of the higher spin decorated parts. In Section V, we present our final discussion and conclusion.

II. MODEL AND METHOD

The TKL XXZ-Ising model has two different kinds of sublattices, which are the a-trimers (the red triangle in FIG.1) and the b-trimers (the blue triangle in FIG.1). In this model, we consider the exchange coupling between the a-spins (the spins in the a-trimers) is of the XXZ type and the coupling between the neighboring a-spins and the b-spins (the spins in the b-trimers) is of the Ising type. The Hamiltonian of the TKL spin-1 model is given by

$$H = -J_a^{xy} \sum_{ai,aj \in a} (S_{ai}^x S_{aj}^x + S_{ai}^y S_{aj}^y) - J_a^z \sum_{ai,aj \in a} S_{ai}^z S_{aj}^z - J_{ab}^z \sum_{ai \in a, bi \in b} S_{ai}^z S_{bi}^z - h \sum_{ai \in a} S_{ai}^z - h \sum_{bi \in b} S_{bi}^z. \quad (1)$$

In which, the spins carry $S = 1/2$ and 1 for the b-spins and the a-spins respectively. The coupling J_{ab}^z between the a-spins and the b-spins is in the z direction. J_a^z (J_a^{xy}) is the couplings of the a-spins in the z (x and y) direction respectively. h is the applied external field. J_a^z , J_a^{xy} , J_{ab}^z and h can be either positive or negative, and we set $|J_{ab}^z|$ to be unit of energy in the following analysis.

In the TKL model, the Hamiltonian can be written as the sum over hexamers which contain six spins (as shown in FIG.2) given by[2]

$$H = \sum_n H_n, \quad (2)$$

$$H_n = -J_a^{xy} \sum_{ai,aj \in a} (S_{ai}^x S_{aj}^x + S_{ai}^y S_{aj}^y) - J_a^z \sum_{ai,aj \in a} S_{ai}^z S_{aj}^z - J_{ab}^z \sum_{ai \in a, bi \in b} S_{ai}^z S_{bi}^z - h \sum_{ai \in a} S_{ai}^z - \frac{h}{2} \sum_{bi \in b} S_{bi}^z. \quad (3)$$

Since the Hamiltonians of different hexamers commute with each other and each a-spin appears in one hexamer but not in the others, it is reasonable to trace over all the a-spins of each hexamer. In consequence, the partition function of each hexamer is the function of the b-spins given by

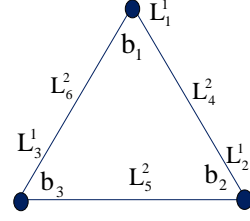


FIG. 3. A trimer after transformation. L_0^0 corresponds to the coefficient of effective background energy, L_1^1 , L_2^2 and L_3^3 correspond to the coefficients of one spin coupling, L_4^4 , L_5^5 and L_6^6 correspond to the coefficients of two spins coupling, L_7^7 correspond to the coefficients of three spin coupling (not shown in the picture).

$$Z(S_{b1}^z, S_{b2}^z, S_{b3}^z) = \text{Tr} e^{-\beta H_n(S_{ai}^z, S_{bi}^z)}. \quad (4)$$

Hence, it is available to transform the hexamer into an effective trimer which only includes the couplings of b-spins (as shown in FIG.3) without changing the partition function of each hexamer or the whole TKL model. According to the general transformation method for the decorated spin systems[19, 20], the Hamiltonian of the effective trimer can be assumed as follows

$$H'_n = -L_0^0 - L_1^1 \sigma_{b1}^z - L_2^2 \sigma_{b2}^z - L_3^3 \sigma_{b3}^z - L_4^4 \sigma_{b1}^z \sigma_{b2}^z - L_5^5 \sigma_{b2}^z \sigma_{b3}^z - L_6^6 \sigma_{b1}^z \sigma_{b3}^z - L_7^7 \sigma_{b1}^z \sigma_{b2}^z \sigma_{b3}^z. \quad (5)$$

Here we use $\sigma_{bi}^z = \pm 1$ for consistency with the Ising model literature. L_0^0 stands for the parameter of the effective background energy. L_1^1 , L_2^2 and L_3^3 represent the coefficients of each b-spin coupling with the effective fields. L_4^4 , L_5^5 and L_6^6 are the coefficients of two b-spins effective couplings. L_7^7 carries the coefficient of three b-spins effective coupling. Since the effective trimer is classical, it is possible to obtain the partition function of each hexamer corresponding to different configurations of the b-spins.

$$Z(\sigma_{b1}^z, \sigma_{b2}^z, \sigma_{b3}^z) = \exp[-\beta H'_n(\sigma_{b1}^z, \sigma_{b2}^z, \sigma_{b3}^z)]. \quad (6)$$

Here $Z(S_{b1}^z, S_{b2}^z, S_{b3}^z) = Z(\sigma_{b1}^z, \sigma_{b2}^z, \sigma_{b3}^z)$ when they share the same b-spin configuration since it is an effective model. As a result, the partition function of the effective trimer is the function of the couplings in each hexamer. To perform the transformation, it is convenient to take the logarithm of both sides of Eq.(6)[19].

$$\ln[Z] = V^{\frac{1}{2}} \otimes V^{\frac{1}{2}} \otimes V^{\frac{1}{2}} \beta L, \quad (7)$$

where

$$\ln[Z] = \begin{pmatrix} \ln[Z(\uparrow\uparrow\uparrow)] \\ \ln[Z(\downarrow\uparrow\uparrow)] \\ \ln[Z(\uparrow\downarrow\uparrow)] \\ \ln[Z(\downarrow\downarrow\uparrow)] \\ \ln[Z(\uparrow\uparrow\downarrow)] \\ \ln[Z(\downarrow\uparrow\downarrow)] \\ \ln[Z(\uparrow\downarrow\downarrow)] \\ \ln[Z(\downarrow\downarrow\downarrow)] \end{pmatrix}, \beta L = \begin{pmatrix} \beta L_0^0 \\ \beta L_3^1 \\ \beta L_2^1 \\ \beta L_2^2 \\ \beta L_5^2 \\ \beta L_1^1 \\ \beta L_1^2 \\ \beta L_6^2 \\ \beta L_4^2 \\ \beta L_7^3 \end{pmatrix}, \quad (8)$$

$$V^{\frac{1}{2}} = \begin{pmatrix} 1 & 1 \\ 1 & -1 \end{pmatrix}, \quad (9)$$

with $(\uparrow\uparrow\uparrow)$, for instance, represents one possible configuration of the b-spins. The effective couplings can be expressed as a function of the original couplings (J_{ab}^z , J_a^z , J_a^{xy} and h) with $(V^{\frac{1}{2}})^{-1} = (V^{\frac{1}{2}})/2$ as follows

$$\beta L = \begin{pmatrix} 1 & 1 & 1 & 1 & 1 & 1 & 1 & 1 \\ 1 & -1 & 1 & -1 & 1 & -1 & 1 & -1 \\ 1 & 1 & -1 & -1 & 1 & 1 & -1 & -1 \\ 1 & -1 & -1 & 1 & 1 & -1 & -1 & 1 \\ 1 & 1 & 1 & 1 & -1 & -1 & -1 & -1 \\ 1 & -1 & 1 & -1 & -1 & 1 & -1 & 1 \\ 1 & 1 & -1 & -1 & -1 & -1 & 1 & 1 \\ 1 & -1 & -1 & 1 & -1 & 1 & 1 & -1 \end{pmatrix} \frac{\ln[Z]}{8}. \quad (10)$$

Specially, in the TKL model, we are able to simplify the effective trimer by making use of its C_3 symmetry ($Z(\downarrow\uparrow\uparrow, h) = Z(\uparrow\downarrow\uparrow, h) = Z(\uparrow\uparrow\downarrow, h)$). Therefore, the effective couplings (or the effective background energy) are given by

$$\begin{aligned} \ln(Z_a) &= \beta L_0^0 \\ &= \ln \left[[Z(\uparrow\uparrow\uparrow, h)Z(\downarrow\downarrow\downarrow, h)]^{\frac{1}{8}} [Z(\downarrow\uparrow\uparrow, h)Z(\uparrow\downarrow\downarrow, h)]^{\frac{3}{8}} \right], \end{aligned} \quad (11)$$

$$\begin{aligned} \beta h_b &= \beta L_1^1 = \beta L_2^1 = \beta L_3^1 \\ &= \frac{1}{8} \ln \left[\frac{Z(\uparrow\uparrow\uparrow, h)Z(\downarrow\uparrow\uparrow, h)}{Z(\downarrow\downarrow\downarrow, h)Z(\uparrow\downarrow\downarrow, h)} \right], \end{aligned} \quad (12)$$

$$\begin{aligned} \beta J_{bb} &= \beta L_4^2 = \beta L_5^2 = \beta L_6^2 \\ &= \frac{1}{8} \ln \left[\frac{Z(\uparrow\uparrow\uparrow, h)Z(\downarrow\downarrow\downarrow, h)}{Z(\downarrow\uparrow\uparrow, h)Z(\uparrow\downarrow\downarrow, h)} \right], \end{aligned} \quad (13)$$

$$\beta J_{bbb} = \beta L_7^3 = \frac{1}{8} \ln \left[\frac{Z(\uparrow\uparrow\uparrow, h)Z(\uparrow\downarrow\downarrow, h)^3}{Z(\downarrow\downarrow\downarrow, h)Z(\downarrow\uparrow\uparrow, h)^3} \right]. \quad (14)$$

Since each b-spin is shared by two hexamers, the effective h_b should be doubled when considering the whole model, leading to the Hamiltonian of the effective trimer being

$$\begin{aligned} H'_n(\sigma_{bi}^z) &= -\ln(Z_a)/\beta - h_b \sum_{bi \in b} \sigma_{bi}^z - J_{bb} \sum_{\langle bi, bj \rangle} \sigma_{bi}^z \sigma_{bj}^z \\ &\quad - J_{bbb} \sum_{\langle bi, bj, bk \rangle} \sigma_{bi}^z \sigma_{bj}^z \sigma_{bk}^z. \end{aligned} \quad (15)$$

With Eq.(15), the TKL spin-1 model can be exactly mapped to the classical kagome model with an extra three-spin coupling. As a result, we can obtain the ground state of the b-spins at zero temperature in the usual manner, which is searching for the lowest energy state of each hexamer[2, 4]. We present the phase diagram and discuss the effect of the interplay between the quantum fluctuations and the geometric frustrations in the TKL spin-1 model in the following sections.

III. ZERO FIELD

A. Mapping to the kagome Ising model

When $h = 0$, the TKL spin-1 model has the time-reversal symmetry ($Z(\uparrow\uparrow\uparrow, h) = Z(\downarrow\downarrow\downarrow, -h)$, $Z(\downarrow\uparrow\uparrow, h) = Z(\uparrow\downarrow\downarrow, -h)$). The Hamiltonian of the effective model can be simplified as

$$H'_n = -\ln(Z_a)/\beta - J_{bb} \sum_{bi, bj \in b} \sigma_{bi}^z \sigma_{bj}^z, \quad (16)$$

in which

$$Z_a = Z(\uparrow\uparrow\uparrow)^{\frac{1}{4}} Z(\downarrow\uparrow\uparrow)^{\frac{3}{4}}, \quad (17)$$

$$\beta J_{bb} = \frac{1}{4} \ln \left[\frac{Z(\uparrow\uparrow\uparrow)}{Z(\downarrow\uparrow\uparrow)} \right], \quad (18)$$

$$\beta h_b = \beta J_{bbb} = 0. \quad (19)$$

After the transformation, the TKL model is mapped to the kagome Ising model exactly, in which all the parameters (J_{bb} and Z_a) are the functions of the original couplings (J_{ab}^z , J_a^z and J_a^{xy}).

B. Free energy and entropy

Since the TKL spin-1 model has been mapped to the kagome Ising model, it is possible to compute the partition function, free energy, internal energy and entropy per unit cell of the TKL spin-1 model with the exact solution of the kagome Ising model[28, 29]. If we define the free energy as $F = \ln(Z)$ for convenience, the free energy of the TKL spin-1 model can be written as a sum of the free energy of the kagome Ising model and a part about the a-trimer free energy, given by

$$f_{\text{TKL}}(J_a^{xy}, J_a^z, J_{ab}^z) = f_b(\beta J_{bb}) + 2f_a, \quad (20)$$

in which $f_a = \ln[Z_a]$. The factor 2 in Eq.(20) comes from the fact that the unit cell of the TKL spin-1 model contains one kagome unit cell and two a-trimers (as shown in FIG.4), which is different from the hexamers.

The internal energy per unit cell can be given by

$$\begin{aligned} u_{\text{TKL}} &= -\frac{df_{\text{TKL}}}{d\beta} \\ &= -\frac{df_b}{d\beta} - 2\frac{df_a}{d\beta} \\ &= u_b + u_a, \end{aligned} \quad (21)$$

where

$$u_a = -2\frac{df_a}{d\beta} = \frac{u_{\uparrow\uparrow\uparrow} + 3u_{\downarrow\uparrow\uparrow}}{2}, \quad (22)$$

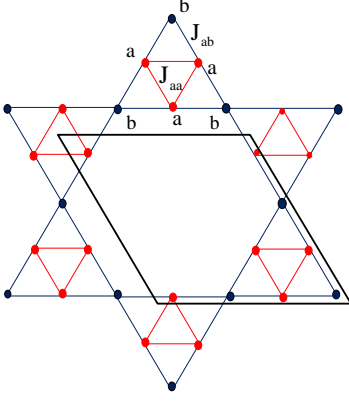


FIG. 4. A unit cell is shown as the blocked area.

and

$$u_b = -\frac{df_b}{d\beta} = \frac{u_{\downarrow\uparrow\uparrow} - u_{\uparrow\uparrow\uparrow}}{4} u_{\text{kag}}(\beta J_{bb}), \quad (23)$$

in which we define $u_{\uparrow\uparrow\uparrow} = [E_{\uparrow\uparrow\uparrow} \exp(-\beta E_{\uparrow\uparrow\uparrow})]/Z$ (and correspondingly, $u_{\downarrow\uparrow\uparrow} = [E_{\downarrow\uparrow\uparrow} \exp(-\beta E_{\downarrow\uparrow\uparrow})]/Z$), which agrees with Ref.[2]. $u_{\text{kag}}(\beta J_{bb})$ is the internal energy per unit cell of the effective kagome Ising model. Finally, the energy per unit cell is

$$u_{\text{TKL}} = \frac{u_{\uparrow\uparrow\uparrow} + 3u_{\downarrow\uparrow\uparrow}}{2} + \frac{u_{\downarrow\uparrow\uparrow} - u_{\uparrow\uparrow\uparrow}}{4} u_{\text{kag}}(\beta J_{bb}). \quad (24)$$

The entropy per unit cell is

$$s_{\text{TKL}} = f_{\text{TKL}} + \beta u_{\text{TKL}}. \quad (25)$$

Since $u_{\uparrow\uparrow\uparrow}$ and $u_{\downarrow\uparrow\uparrow}$ are dominated by the lowest energy of each hexamer at zero temperature (as shown in FIG.5), we can compute the free energy and entropy of the TKL spin-1 model with the exact solutions of the kagome Ising model[28–30]. In addition, βJ_{bb} serves as an important part in the effective model since it is one of the determining parameters in the kagome Ising model.

C. Phase diagram at zero temperature and ground state properties

When $T \rightarrow 0$, βJ_{bb} becomes

$$\beta J_{bb} = \frac{1}{4} \left[\ln \left(\frac{D_1}{D_2} \right) + \beta [E_0(\downarrow\uparrow\uparrow) - E_0(\uparrow\uparrow\uparrow)] \right]. \quad (26)$$

Here, $E_0(\uparrow\uparrow\uparrow)(E_0(\downarrow\uparrow\uparrow))$ and $D_1(D_2)$ denote the ground state energy and the ground state degeneracy of each a-trimer when the b-spin configuration is $(\uparrow\uparrow\uparrow)(\downarrow\uparrow\uparrow)$ at zero temperature respectively. In addition, we define D for the degeneracy of each hexamer in the following analysis.

When βJ_{bb} is positive, the effective model is a kagome Ising model with ferromagnetic coupling. The long range order of the b-spins depends on the relation between βJ_{bb} and

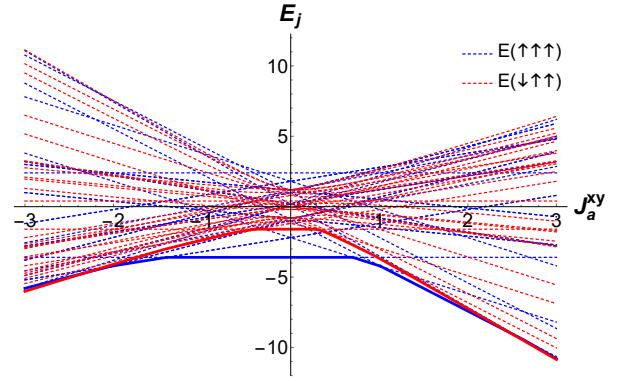


FIG. 5. The energy level of each hexamer when the b-spin configuration is $(\uparrow\uparrow\uparrow)$, dotted blue line) or $(\downarrow\uparrow\uparrow)$, dotted red line) with $J_a^z = 0.2$, $J_{ab}^z = -1$, $h = 0$ and different J_a^{xy} in FIG.5. We also highlight the lowest ground state energy level of each b-spin configuration with the full lines.

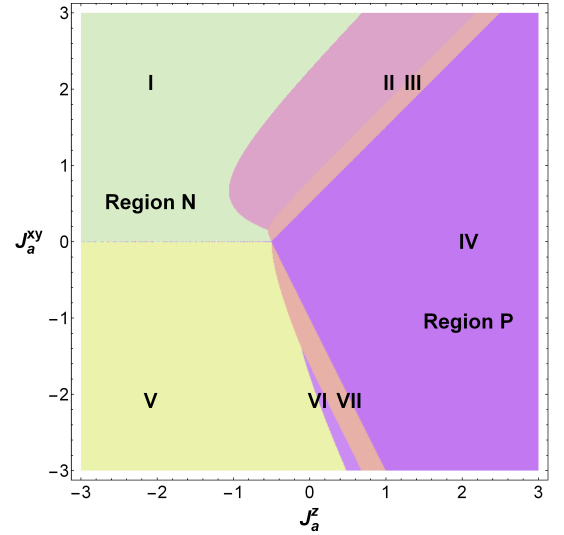


FIG. 6. Phase diagram at $T = 0$ is identified by the energy of each hexamer when $h = 0$ and $J_{ab}^z = -1$. The phase diagram is divided into two main regions by the sign of βJ_{bb} , which we denote as Region P (for βJ_{bb} is positive) and Region N (for βJ_{bb} is negative). We mark the phases in Region N as I and V and the phases in Region P as II, III, IV, VII and VI.

the critical point of the ferromagnetic kagome Ising model $\beta J_{\text{kag}} = (\ln[3 + \sqrt{12}])/4$ [29]. For negative βJ_{bb} , the effective model can be regarded as an isotropic antiferromagnetic kagome Ising model, which is disorder at all temperature due to its geometric frustrations[28].

We present the phase diagram at zero temperature in FIG.6. The phase diagram can be divided into two regions by the sign of βJ_{bb} , which are marked as Region P and Region N in FIG.6. The boundaries between two regions are represented as BL:II, BL:III and BL:IV (seen in TABLE.II) according to the phases on each side of them. TABLE.II shows the entropies of these phase boundaries at zero temperature. Note that the BP:I has the highest entropy, which satisfy the intuition that the entropy

TABLE I. The effective βJ_{bb} , S_{atot}^z and degeneracy D of each phase for $h = 0$ at zero temperature.

	βJ_{bb}	S_{atot}^z	D	Phase
Region N	$-\infty$			Anti-Ferromagnetic Phase
Region N Including:				
Phase I	$-\infty$	0	1	Anti-Ferromagnetic Phase
Phase V	$-\infty$	0	2	Anti-Ferromagnetic Phase
Region P	∞			Ferrimagnetic Phase
Region P Including:				
Phase II	∞	-1	1	Ferrimagnetic Phase
Phase III	∞	-2	1	Ferrimagnetic Phase
Phase IV	∞	-3	1	Ferrimagnetic Phase
Phase VI	∞	-1	2	Ferrimagnetic Phase
Phase VII	∞	-2	2	Ferrimagnetic Phase

TABLE II. The βJ_{bb} and entropy per site of the TKL model for phase boundaries when $h = 0$ at zero temperature. All of them have the finite correlation length

Boundary	Boundary About	βJ_{bb}	$s_0/9$
BL:I	Phase I and Phase V	$(1/4) \ln(3/5)$	0.407945
BL:II	Phase I and Phase II	0	0.231049
BL:III	Phase V and Phase VI	$(1/4) \ln 2$	0.280644
BL:IV	Phase V and Phase VII	$(1/4) \ln 2$	0.280644
BP:I	Phase I, V and IV	$(1/4) \ln(7/5)$	0.609883
BP:II	Phase V, VI and VII	$(1/4) \ln 4$	0.356169

of a system at transition line or dot should be higher than that of the surrounding phases.

In addition, there are several different phases in each region corresponding to different states of the a-trimers, which can be identified by calculating

$$S_{\text{atot}}^z = \sum_{\text{ai} \in \alpha} S_{\text{ai}}^z, \quad (27)$$

in which S_{ai}^z stands for the a-spins in the same hexamer. Since $[S_{\text{atot}}^z, H] = 0$, S_{atot}^z is compatible with the Hamiltonian of the TKL spin-1 model.

In Region P, the ground state energies of each hexamer obey $E_0(\uparrow\uparrow\uparrow) < E_0(\downarrow\uparrow\uparrow)$, which causes βJ_{bb} to tend to infinity. Hence the b-spins have perfect ferromagnetic long-range order. However, with $S_{\text{atot}}^z < 0$, the TKL spin-1 model is in the ferrimagnetic phases. Moreover, this region is divided into five phases corresponding to different states of the a-trimers, and the entropy in phase IV is zero at zero temperature.

The ground state energies obey $E_0(\uparrow\uparrow\uparrow) > E_0(\downarrow\uparrow\uparrow)$ in Region N, meaning that βJ_{bb} tends to negative infinity. It leads to an antiferromagnetic phase at zero temperature[4]. This region can also be divided into two phases but both of them correspond to $S_{\text{atot}}^z = 0$.

In the boundaries between Region P and Region N, the ground state energies are equal, $E_0(\uparrow\uparrow\uparrow) = E_0(\downarrow\uparrow\uparrow)$. In fact, $E_0(\uparrow\uparrow\uparrow)$ and $E_0(\downarrow\uparrow\uparrow)$ can also be equal in BL:I, BP:I and BP:II, which are presented in TABLE.II. The value of βJ_{bb} depends on the ratio of the degeneracies D_1/D_2 . For different boundaries, the ratios of the degeneracies are different and the

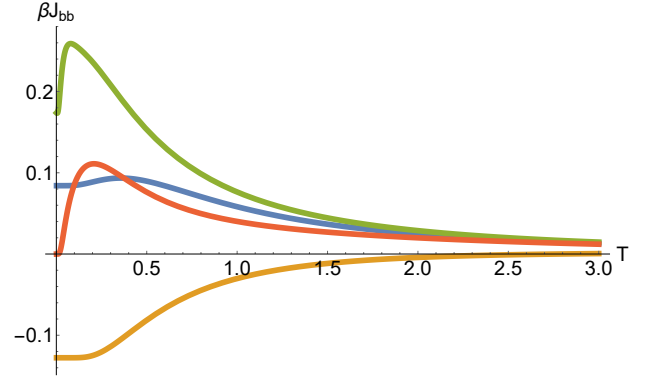


FIG. 7. The effective βJ_{bb} does not go to infinity in some special point at $T = 0$. The blue line is for $J_a^z = -0.5$, $J_a^{xy} = 0$, the orange one is for $J_a^z = -3$, $J_a^{xy} = 0$, the red one is for $J_a^z = -0.223591$, $J_a^{xy} = 2$, the green one is for $J_a^z = -0.259402$, $J_a^{xy} = -1$.

possible values of βJ_{bb} are finite but can be positive (BL:III, BL:IV, BP:I, BP:II) and negative (BL:I) or even zero (BL:II), as presented in FIG.7. For nonnegative βJ_{bb} , whether the b-spins have long-range order depends on whether the effective coupling βJ_{bb} exceeds the critical coupling of the kagome Ising model $\beta J_{\text{kag}} = [\ln(3 + \sqrt{12})]/4$ [29]. Beside, there are high degeneracies for each hexamer in the phase boundaries. Among them, BP:I at $J_a^z = -0.5$ and $J_a^{xy} = 0$ has the highest degeneracy, which leads to its outstanding zero temperature entropy. It has twelve degenerate energy levels including seven of which have the b-spin configuration ($\uparrow\uparrow\uparrow$) and five of which have ($\downarrow\uparrow\uparrow$).

The phase diagram of the TKL spin-1 model at zero temperature presents an outstanding diversity of the magnetization properties corresponding to different orders of the b-spins and different states of the a-trimers.

D. Physical explanation and comparison with the TKL spin-1/2 model

To explain the diversity of the phase diagram, we consider $J_a^{xy} = 0$ first. When J_a^z increases, there is a phase transition point about the disorder phase and the ferrimagnetic phase (the b-spin configuration ($\uparrow\uparrow\uparrow$) and $S_{\text{atot}}^z = -3$) as shown in FIG.6. The critical point is given by $J_a^z = -0.5$. Each hexamer is non-degenerate in the ferrimagnetic phase while its degeneracy is $D = 8$ in the disordered phase in which the b-spin configuration ($\uparrow\uparrow\uparrow$) contributes $D = 3$ and ($\downarrow\uparrow\uparrow$) donates $D = 5$. Although the three degenerate states in ($\uparrow\uparrow\uparrow$) share the same $S_{\text{atot}}^z = -1$, the five degenerate states in ($\downarrow\uparrow\uparrow$) contain different $S_{\text{atot}}^z = \pm 1, 0$.

However, the degeneracy of each hexamer at the critical point is twelve and higher than the sum of the degeneracies in the disordered phase and the ferrimagnetic phase, which contains seven in ($\uparrow\uparrow\uparrow$) and five in ($\downarrow\uparrow\uparrow$). This difference is due to the presence of a new state ($\uparrow\uparrow\uparrow$) with $S_{\text{atot}}^z = -2$ at the critical point.

The presence of J_a^{xy} leads to new phases, which mainly re-

sult from that the classically degenerate states of each a-trimer become stable quantum ground states[4] under the perturbation of J_a^{xy} . We present such effect in each hexamer with each configuration of the b-spins in FIG.8. However, J_a^{xy} also influences the effective coupling βJ_{bb} , which determines the ground state configuration of the b-spins. Therefore, the phase diagram of the TKL spin-1 model becomes complicated and diversified.

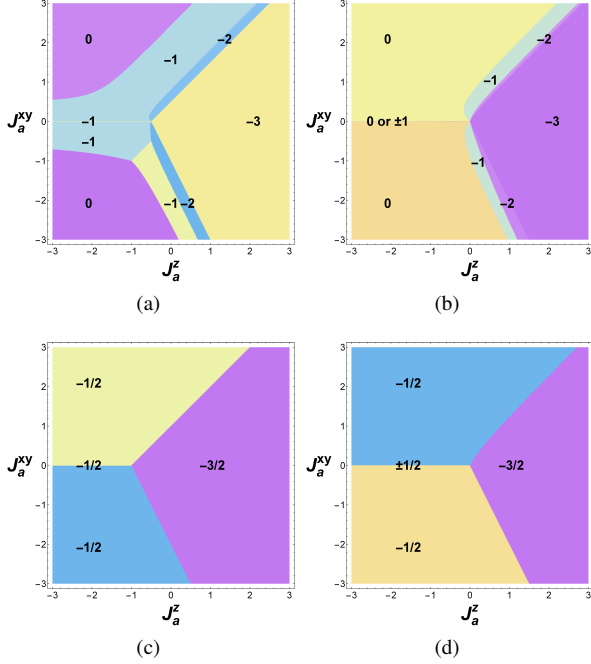


FIG. 8. S_{atot}^z becomes variant in each hexamer with different configurations of the b-spins as J_a^{xy} increases. (a) is for the b-spin configuration ($\uparrow\uparrow\uparrow$) while (b) is for ($\downarrow\uparrow\uparrow$). When $J_a^{xy} = 0$, S_{atot}^z when ($\downarrow\uparrow\uparrow$) has richer values since a-trimer can be regarded as being affected by an anisotropic effective field. We also present the spin-1/2 cases, where (c) (d) has the same configuration of the b-spins as in (a) (b). S_{atot}^z in the spin-1 case has richer values compared to the spin-1/2 case.

As J_a^{xy} increases, the energy degeneracy in the disordered phase between ($\uparrow\uparrow\uparrow$) and ($\downarrow\uparrow\uparrow$) vanishes, and ($\downarrow\uparrow\uparrow$) with $S_{\text{atot}}^z = 0$ is favored due to its lower ground state energy. Moreover, the new state above ($\uparrow\uparrow\uparrow$) with $S_{\text{atot}}^z = -2$) becomes a stable phase while it only appears at the critical point in the classical limit ($J_a^{xy} = 0$). In consequence, as J_a^z increases, the TKL spin-1 model changes from the anti-ferromagnetic phase with $S_{\text{atot}}^z = 0$ to the ferrimagnetic phase with $S_{\text{atot}}^z = -1$. Then, in the ferrimagnetic phase, S_{atot}^z of each hexamer decreases from -1 to -3 . Finally, the TKL spin-1 model is in the ferrimagnetic phase with $S_{\text{atot}}^z = -3$

Comparing with the TKL spin-1/2 model, the TKL spin-1 model has a more diversified phase diagram since the richer quantum ground states of the a-trimers. In the TKL spin-1/2 model, there is no significant difference for S_{atot}^z between $J_a^{xy} = 0$ and $J_a^{xy} \neq 0$. However, in the spin-1 case, the possible values of S_{atot}^z stay at $0, -1$ and -3 when $J_a^{xy} = 0$. As J_a^{xy} increases, S_{atot}^z becomes $0, -1, -2$ and -3 . Eventually, the phase diagram becomes more diversified when combining

with the competition between different b-spin configurations.

IV. FINITE EXTERNAL FIELD IN THE ZERO TEMPERATURE LIMIT

A. Mapping to the kagome Ising model with the three-spin coupling

We now consider the TKL spin-1 model with a finite magnetic field, which is parallel to the axis of the b-spins. The transformation method above is also applicable to this case. As a result of the time-reversal symmetry breaking, the odd spin effective coupling terms in the effective Hamiltonian cannot vanish and the effective Hamiltonian of each hexamer is more complicated

$$H'_n = -\ln(Z_a)/\beta - J_{bb} \sum_{\text{bi,bj} \in b} \sigma_{\text{bi}}^z \sigma_{\text{bj}}^z - J_{bbb} \sum_{\text{bi,bj,bk} \in b} \sigma_{\text{bi}}^z \sigma_{\text{bj}}^z \sigma_{\text{bk}}^z - h_b \sum_{\text{bi} \in b} \sigma_{\text{bi}}^z, \quad (28)$$

in which

$$Z_a = [Z(\uparrow\uparrow\uparrow, h)Z(\downarrow\downarrow\downarrow, h)]^{\frac{1}{8}} [Z(\downarrow\uparrow\uparrow, h)Z(\uparrow\downarrow\downarrow, h)]^{\frac{3}{8}}, \quad (29)$$

$$\beta J_{bb} = \frac{1}{8} \ln \left[\frac{Z(\uparrow\uparrow\uparrow, h)Z(\downarrow\downarrow\downarrow, h)}{Z(\downarrow\uparrow\uparrow, h)Z(\uparrow\downarrow\downarrow, h)} \right], \quad (30)$$

$$\beta J_{bbb} = \frac{1}{8} \ln \left[\frac{Z(\uparrow\uparrow\uparrow, h)Z(\uparrow\downarrow\downarrow, h)^3}{Z(\downarrow\downarrow\downarrow, h)Z(\downarrow\uparrow\uparrow, h)^3} \right], \quad (31)$$

$$\beta h_b = \frac{1}{8} \ln \left[\frac{Z(\uparrow\uparrow\uparrow, h)Z(\downarrow\uparrow\uparrow, h)}{Z(\downarrow\downarrow\downarrow, h)Z(\uparrow\downarrow\downarrow, h)} \right]. \quad (32)$$

In this case, the new parameters in the effective model (Z_a , h_b , J_{bb} and J_{bbb}) are the functions of the original couplings in the TKL spin-1 model (J_{ab}^z , J_a^z , J_a^{xy} and h) after transformation.

B. Phase diagram at zero temperature and ground states properties

Although the odd spin couplings make it hard to obtain a rigorous solution of the model, it is still possible to deduce a full phase diagram of the TKL spin-1 model at zero temperature since its effective model is classical[2, 4]. The phase diagram can be achieved in the usual manner by searching for the b-spin configurations of each hexamer has the lowest energy. The energy of each b-spin configuration is

$$E(\uparrow\uparrow\uparrow) = -\ln(Z_a)/\beta - 3J_{bb} - J_{bbb} - 3h_b, \quad (33)$$

$$E(\downarrow\downarrow\downarrow) = -\ln(Z_a)/\beta - 3J_{bb} + J_{bbb} + 3h_b, \quad (34)$$

TABLE III. The energy of the hexamers at some points in each phase with $J_a^z = J_a^{xy}$, $J_{ab}^z = -1$ and different h in FIG.9b. We also highlight (the underline numbers) which configuration of b-spins has the lowest energy in each phase at zero temperature.

Phase	$J_a^{xy} = J_a^z$	h	$E(\uparrow\uparrow\uparrow)$	$E(\downarrow\uparrow\uparrow)$	$E(\downarrow\downarrow\downarrow)$	$E(\uparrow\downarrow\downarrow)$
Phase I	-3	1	<u>-9.75</u>	-9.46005	-8.25	-8.96005
Phase II	-2	3.552	<u>-9.216</u>	-9.03515	-6.44	-7.664
Phase III	-1.184	3.856	<u>-8.604</u>	-8.39904	-8.124	-8.052
Phase IV	5	5	<u>-30.75</u>	-30.25	-29.25	-29.75
Phase V	-1.2	3.4	-7.35	<u>-7.37237</u>	-7.05	-6.95
Phase VI	2	2	-10.5	-11.5	<u>-13.5</u>	-12.5
Phase VII	-1	1.2	-3.9	<u>-4.16246</u>	-3.5	-3.9
Phase VIII	-1	0.3	-3.225	<u>-3.55619</u>	-3.075	-3.40619
Phase IX	-0.64	0.544	-2.328	-2.67641	-2.68	<u>-2.688</u>
Phase X	-0.48	0.32	-1.88	-2.19117	<u>-2.4</u>	-2.2

TABLE IV. Each phase in FIG.9 identified by calculating the configuration of b-spins and S_{atot}^z in the ground state of each hexamer.

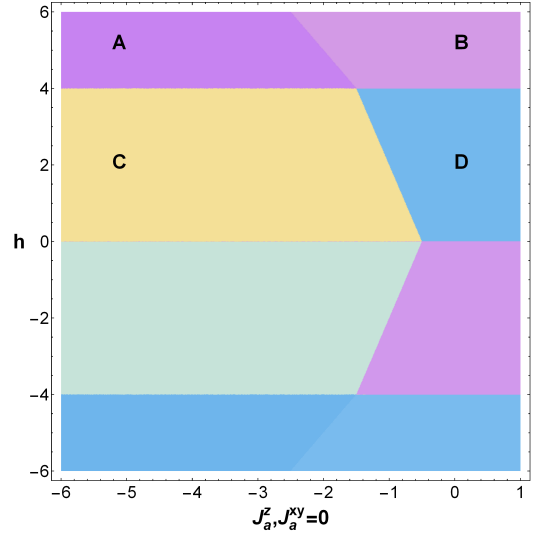
Phase Mark	b-spins	S_{atot}^z	D	Phase
$J_a^{xy} = 0 \quad J_{ab}^z = -1$				
Phase A	$\uparrow\uparrow\uparrow$	1	3	Ferrimagnet
Phase B	$\uparrow\uparrow\uparrow$	3	1	Saturated Ferromagnet
Phase C	$\downarrow\downarrow\downarrow$	1	1	Honeycomb Dimer Liquid
Phase D	$\downarrow\downarrow\downarrow$	3	1	Ferrimagnet
$J_a^z = J_a^{xy} \quad J_{ab}^z = -1$				
Phase I	$\uparrow\uparrow\uparrow$	0	1	Ferrimagnet
Phase II	$\uparrow\uparrow\uparrow$	1	3	Ferrimagnet
Phase III	$\uparrow\uparrow\uparrow$	2	2	Ferrimagnet
Phase IV	$\uparrow\uparrow\uparrow$	3	1	Saturated Ferromagnet
Phase V	$\downarrow\downarrow\downarrow$	2	2	Honeycomb Dimer Liquid
Phase VI	$\downarrow\downarrow\downarrow$	3	1	Ferrimagnet
Phase VII	$\downarrow\uparrow\uparrow$	1	1	Honeycomb Dimer Liquid
Phase VIII	$\downarrow\uparrow\uparrow$	0	1	Honeycomb Dimer Liquid
Phase IX	$\downarrow\downarrow\uparrow$	1	1	Honeycomb Dimer Liquid
Phase X	$\downarrow\downarrow\downarrow$	2	2	Ferrimagnet

$$E(\downarrow\uparrow\uparrow) = -\ln(Z_a)/\beta + J_{bb} + J_{bbb} - h_b, \quad (35)$$

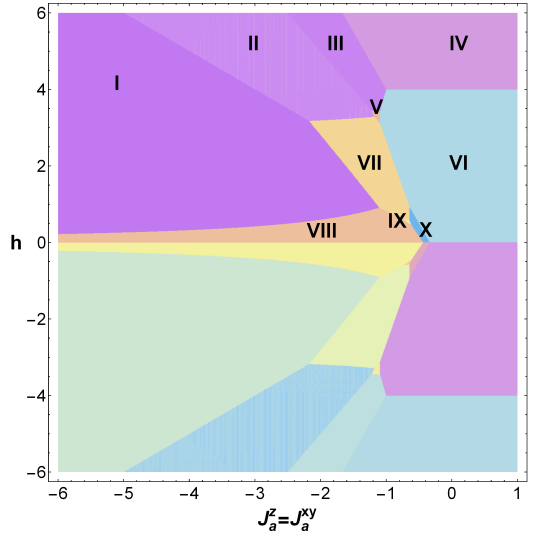
$$E(\uparrow\downarrow\downarrow) = -\ln(Z_a)/\beta + J_{bb} - J_{bbb} + h_b. \quad (36)$$

Here, we obtain the ground state of the TKL spin-1 model by finding the ground state of each hexamer numerically for each combination of parameters. When the ground state energy of the b-spin configuration ($\uparrow\uparrow\uparrow$) or ($\downarrow\downarrow\downarrow$) is favored, the TKL spin-1 model is in ferromagnetic phase or ferrimagnetic phase, which is depended on the a-trimer states. For the ($\downarrow\uparrow\uparrow$) or ($\uparrow\downarrow\downarrow$) cases, the macroscopic ground state of its effective model can be achieved by enumerating the ways of tilling the corresponding effective trimers in the kagome plane, which is equivalent to placing dimers on the bonds of a honeycomb lattice[2, 4].

Figure.9 shows the phase diagram when $J_a^{xy} = 0$, $J_{ab}^z = -1$ (FIG.9a) and $J_a^z = J_a^{xy}$, $J_{ab}^z = -1$ (FIG.9b) at zero temperature. TABLE.III lists the ground state energy of each hexamer at selected points in each phase in FIG.9b. The phase diagram is divided into eight parts when $J_a^{xy} = 0$ but twenty in the $J_a^z = J_a^{xy}$ case, and both of them are symmetric about $h = 0$.



(a) $J_a^{xy} = 0$, $J_{ab}^z = -1$



(b) $J_a^z = J_a^{xy}$, $J_{ab}^z = -1$

FIG. 9. The phase diagram of the TKL model with spin-1 at zero temperature identified by calculating the energy of each hexamer when the TKL spin-1 model is in its classical limit ($J_a^{xy} = 0$, $J_{ab}^z = -1$ and $T = 0$) and Heisenberg limit ($J_a^z = J_a^{xy}$, $J_{ab}^z = -1$ and $T = 0$).

The phase diagram in the classical limit is similar to the TKL model with spin-1/2 trimers[2], while the Heisenberg limit is quite different, including the absence of the kagome loop gas phase[2] and the presence of some unstable phases (phase V, phase IX and phase X)

C. Physical explanation and the effect of the a-trimer quantum fluctuations

To explain how the unstable phases come from the quantum fluctuations of the a-trimers, we first focus on the classical limit. The phase diagram in the classical limit is divided

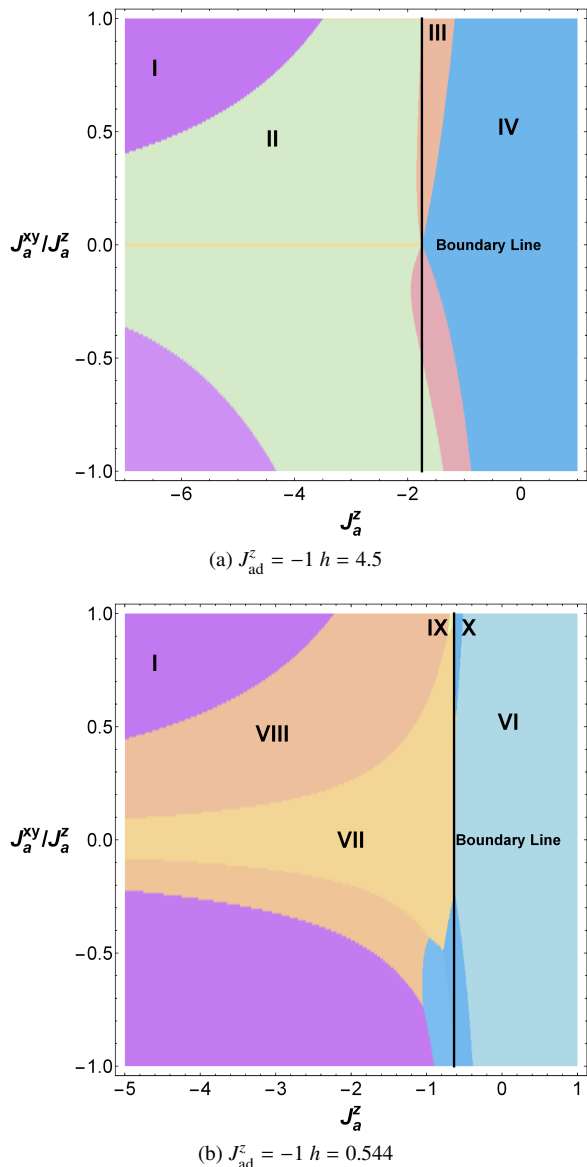


FIG. 10. These figures show the phases changing as J_a^{xy}/J_a^z increases from 0 to 1. These phase marks here are same as in FIG.9b. $J_{ad}^z = -1$ and $h = 4.5$ in FIG.10a while $J_{ad}^z = -1$ and $h = 0.544$ in FIG.10b, which is crossing through the unstable phase IX. The boundary line in the figures is crossing through the transition point in the classical limit with the same values of J_{ad}^z . These figures present a better view of how new phases emerge.

into four different phases when h is positive, including saturated ferromagnetic phase (Phase B), ferromagnetic phase with $S_{\text{atot}}^z = 1$ (Phase A), ferrimagnetic phase with $S_{\text{atot}}^z = 3$ (Phase D) and honeycomb dimer phase (Phase C), which is quite similar to the TKL spin-1/2 model[2]. It is possible to identify the boundary conditions as $2J_a^z + h = 1$ for the boundary between Phase A and Phase B, $h = 4$ for the boundary between Phase A and Phase C or between Phase B and Phase D, $h + 4J_a^z = -2$ for the boundary between Phase C and Phase D.

To observe how the quantum fluctuations in the a-trimers

influence the phase diagram, it is useful to consider the phase diagram at zero temperature with fixed h , J_{ab}^z and parameters J_a^{xy}/J_a^z and J_a^z , which demonstrates the effect of J_a^{xy} more directly. We present the new phase diagrams with $J_{ad}^z = -1$ and $h = 4.5$ in FIG.10a and $J_{ad}^z = -1$ and $h = 0.544$ in FIG.10b. The former contains stable phases while the later includes the most unstable phase (phase IX) in its Heisenberg limit ($J_a^z = J_a^{xy}$)

In FIG.10a, the TKL spin-1 model changes into phase IV ($(\uparrow\uparrow\uparrow)$ with $S_{\text{atot}}^z = 3$ without degeneracy) directly as J_a^z increases in the classical limit ($J_a^{xy} = 0$). When J_a^{xy}/J_a^z increases from zero, there is a new phase emerging with the b-spin configuration ($\uparrow\uparrow\uparrow$) and $S_{\text{atot}}^z = 2$. This new phase emerges from the critical point in its classical limit. It stays around the boundary line, which is crossing through the critical point as shown in FIG.10a. Another new phase emerges with the b-spin configuration ($\uparrow\uparrow\uparrow$) and smaller $S_{\text{atot}}^z = 0$ from the negative side of the phase diagram. Eventually, the S_{atot}^z of each hexamer change from 0 to 1 and then to 2 finally to 3 with the same b-spin configuration in its Heisenberg limit, which leads to a quantized growth of the magnetization process when J_a^{xy} increase. All these phases at each side of the boundary line share the same configuration of the b-spins, which means the a-trimers does not influence the ground state of the effective model yet. In other words, the phase transitions between these phases is only about the ground state transition of each a-trimer and have nothing to do with the effective model. As a result, these new phases are stable.

However, in the boundary between phase VI and phase VII in the classical limit (FIG.10b), the situation is more complicated since the a-trimers also make a difference on the ground state of the effective model. In the classical limit, the TKL spin-1 model has a phase transition from phase VII (the honeycomb dimer liquid phase) to phase VI (the ferrimagnet phase) directly when J_a^z increases. We also set a boundary line crossing through the critical point in the classical limit (as shown in FIG.10b). When J_a^{xy} appears, there are two new phases emerging from the negative side, which are phase I ($(\uparrow\uparrow\uparrow)$ with $S_{\text{atot}}^z = 0$) and phase VIII ($(\downarrow\uparrow\uparrow)$ with $S_{\text{atot}}^z = 0$). When J_a^{xy}/J_a^z becomes larger, phase I and phase VIII come closer to the boundary line and a new phase X ($(\downarrow\downarrow\downarrow)$ with $S_{\text{atot}}^z = 2$) emerges on the left side of the boundary line. When J_a^{xy}/J_a^z is larger, the quantum fluctuations of the a-trimers finally affect the ground state b-spin configuration and lead to a new phase IX ($(\downarrow\downarrow\uparrow)$ with $S_{\text{atot}}^z = 1$), which is hard to obtain in the classical limit. Finally, when J_a^z increases in the Heisenberg limit ($J_a^{xy} = J_a^z$), the b-spin configuration of each hexamer changes from ($\downarrow\uparrow\uparrow$) to ($\downarrow\downarrow\uparrow$) and then to ($\downarrow\downarrow\downarrow$). It is reasonable since the effective coupling J_{bb} is negative and the phase transition between two opposite polar phases is possible topologically[2].

D. Comparison with the TKL spin-1/2 model and discussion of the TKL higher spin model

We now compare the phase diagram of the TKL spin-1 model with the spin-1/2 case and find that the TKL spin-

1 model has a much more diversified phase diagram at zero temperature. These differences mainly come from the richer possible states of the a-trimers under the effect of quantum fluctuations.

In the classical limit, there are four main phases both in the spin-1/2 and in the spin-1 cases, including the Saturated Ferrimagnet phase ($\uparrow\uparrow\uparrow$), the Honeycomb Dimer Liquid phase ($\downarrow\uparrow\uparrow$), the Ferrimagnet phase ($\uparrow\uparrow\downarrow$) and the Ferrimagnet phase ($\downarrow\downarrow\downarrow$). When J_a^{xy} appears, these four main phases are divided into more phases because of the quantum fluctuations of the a-trimers. Since there are more possible states of the a-trimers in the TKL spin-1 model than in the spin-1/2 case, the phase diagram is divided into more phases. In consequence, the TKL spin-1 model has much more diversified magnetization properties in its Heisenberg limit due to the diversify of the a-trimer states. Such effect can also happen in the Heisenberg-Ising diamond chain [1, 5].

Although it is hard to give an exact picture of how the phase diagram of the TKL model changes when the spins in the a-trimers tend to infinity, it is still possible to give a simple description of it. First, the four main phases above are present in the classical limit of the TKL model in higher spin cases. In its Heisenberg limit, these phases still remain while being affected by the quantum fluctuations of the a-trimers. Besides, more new phases with different a-trimer states emerge when J_a^{xy} increases if we consider higher spins in the a-trimers. This is due to the richer possible states of the a-trimers under the effect of the quantum fluctuations. Moreover, these new phases emerge around the phase boundaries of its classical limit. When considering higher and higher spins in the a-trimers, some of these new phases may appear more and more compactly around the boundaries. Eventually, if the spins tend to infinity, some of them may become a line or dot with high degeneracy and the phase diagram in the Heisenberg limit at zero temperature should approach its classical limit.

V. CONCLUSION

In conclusion, we have discussed the TKL XXZ-Ising model decorated by the spin-1 a-trimers and computed its phase diagram by transforming into an effective kagome Ising model with or without the three-spin coupling according to the presence of the finite external field. The transformation method is an essentially algebraic method and can be applied even in more general cases. For $h = 0$, the effective model can be simplified with the $C3$ symmetry and the time-

reversal symmetry, and the TKL spin-1 model is mapped to the kagome Ising model exactly. In the zero temperature phase diagram, there are two main regions corresponding to the b-spin configurations ($\uparrow\uparrow\uparrow$) and ($\downarrow\uparrow\uparrow$) respectively, which can help us deduce the ground states of the whole model. Each main region can be divided into several phases corresponding to different states of the a-trimers. Compared to the TKL spin-1/2 model, the phase diagram of the spin-1 case is more diversified since the richer possible a-trimer states under the effect of quantum fluctuations.

When considering a finite external field, only the $C3$ symmetry can be applied to simplify the effective model, which means that we can map the TKL spin-1 model to the kagome Ising model with the three-spin coupling. Fortunately, the phase diagram at zero temperature can be obtained because its effective model is classical[2, 4, 31]. For the classical limit ($J_a^{xy} = 0$), there are four main phases, which is similar to the TKL spin-1/2 case. However, in the presence of J_a^{xy} , the phases of the TKL spin-1 model can be divided into more phases than that of the spin-1/2 case. Finally, in the Heisenberg limit ($J_a^{xy} = J_a^z$), it has a much more diversified phase diagram than the TKL spin-1/2 model.

The higher spin for the decorated a-trimers can give a larger dimension of Hilbert spaces. In the spin-1/2 case, the possible values of S_{atot}^z are $\pm 1/2$ and $\pm 3/2$ in both the classical limit and the Heisenberg limit. However, in the spin-1 case, the possible values of S_{atot}^z are ± 1 and ± 3 in the classical limit but $0, \pm 1, \pm 2$ and ± 3 in the Heisenberg limit. This leads to more plentiful states for the a-trimers and more complicated effective couplings. Therefore, the phase diagram becomes more diversified for the TKL spin-1 model compared with the spin-1/2 case. This is a strong evidence that the quantum fluctuations can create new phases in the highly frustrated spin systems, and helps to understand how the XXZ-Ising decorated model evolves to its classical limit when S increases for the decorated spins.

ACKNOWLEDGMENTS

We thank E. W. Carlson, Y. L. Loh, Y. -R. Shu, and M. Lake for useful discussions. This project is supported by NKRDPC-2017YFA0206203, NSFC-11574404, NSFC-11275279, NSFG-2015A030313176, Special Program for Applied Research on Super Computation of the NSFC-Guangdong Joint Fund, Leading Talent Program of Guangdong Special Projects.

-
- [1] K. Takano, K. Kubo, and H. Sakamoto, *Journal of Physics: Condensed Matter* **8**, 6405 (1996).
 - [2] D. X. Yao, Y. L. Loh, E. W. Carlson, and M. Ma, *Phys. Rev. B* **78**, 024428 (2008).
 - [3] C. Lhuillier and G. Misguich, *arXiv: Strongly Correlated Electrons*, 161 (2001).
 - [4] R. Moessner, S. L. Sondhi, and P. Chandra, *Phys. Rev. Lett.* **84**, 4457 (1999).
 - [5] L. Canova, J. Strecka, and T. Lucivjansky, *Condensed Matter Physics* **12**, 353 (2009).
 - [6] S. Maruti and L. W. ter Haar, *J. Appl. Phys.* **75**, 5949 (1994).
 - [7] M. Gonzalez, F. Cervantes-lee, and L. W. ter Haar, *Mol. Cryst. Liq. Cryst. Sci. Technol.* **233**, 317 (1993).
 - [8] S. Ateca, S. Maruti, and L. W. T. Haar, *J. Magn. Magn. Mater.* **147**, 398 (1995).
 - [9] M. Isoda, H. Nakano, and T. Sakai, *J. Phys. Soc. Jpn.* **81**,

- 053703 (2012).
- [10] R. Moessner, S. L. Sondhi, and P. Chandra, *Physical Review Letters* **84**, 4457 (2000).
- [11] R. Moessner and S. L. Sondhi, *Physical Review B* **63**, 224401 (2001).
- [12] R. Moessner and S. L. Sondhi, *Physical Review B* **68**, 064411 (2003).
- [13] Y. L. Loh, D. X. Yao, and E. W. Carlson, *Phys. Rev. B* **78**, 224410 (2008).
- [14] J. Zheng and G. Sun, *Phys. Rev. B* **71** (2005).
- [15] D. Yamamoto, G. Marmorini, and I. Danshita, *Physical Review Letters* **112**, 127203 (2014).
- [16] Y. L. Loh, D. X. Yao, and E. W. Carlson, *Phys. Rev. B* **77**, 134402 (2007).
- [17] J. Strecka, L. Canova, M. Jascur, and M. Hagiwara, *Phys. Rev. B* **78**, 024427 (2008).
- [18] M. E. Fisher, *Phys. Rev.* **113**, 969 (1959).
- [19] O. Rojas, J. S. Valverde, and S. M. De Souza, *Physica A* **388**, 1419 (2009).
- [20] J. Strecka, *Phys. Lett. A* **374**, 3718 (2010).
- [21] D. A. Antonosyan, S. Bellucci, and V. Ohanyan, *Phys. Rev. B* **79** (2008).
- [22] L. Galisova, *Phys. Status Solidi B* **250**, 187 (2013).
- [23] N. Ananikian, J. Strecka, and V. Hovhannisyanyan, *Solid State Commun.* **194**, 48 (2014).
- [24] J. Oitmaa and M. Keppert, *J. Phys. A* **35**, L219 (2002).
- [25] S. Hanks, T. Datta, and J. Oitmaa, *Phys. Rev. E* **87**, 062143 (2013).
- [26] S. Chunfeng, K. Xiangmu, and Y. Xunchang, *Commun. Theor. Phys.* **45**, 555 (2006).
- [27] J. Riedler, *arXiv: High Energy Physics - Lattice* (1993).
- [28] K. Kano and S. Naya, *Prog. Theor. Phys.* **10**, 158 (1953).
- [29] I. Syozi, *Progr. Theor. Exp. Phys.* **6**, 306 (1951).
- [30] “Two-dimensional frustrated ising systems,” in *Statistical Mechanics of Periodic Frustrated Ising Systems* (Springer Berlin Heidelberg, Berlin, Heidelberg, 1986) pp. 26–108.
- [31] H. Ishikawa, T. Okubo, Y. Okamoto, and Z. Hiroi, *J. Phys. Soc. Jpn.* **83**, 043703 (2014).